







Cite this: *RSC Adv.*, 2020, 10, 27235

Enhancing the water splitting performance *via* decorating Co₃O₄ nanoarrays with ruthenium doping and phosphorization†

Jiaqi Niu, ^a Jian Yang, ^a Ali Imran Channa, ^b Eric Ashalley, ^b Jiachao Yang,^a Jie Jiang,^a Handong Li,^a Haining Ji^{*a} and Xiaobin Niu ^{*a}

Hydrogen is the most promising renewable energy source to replace traditional fossil fuels for its ultrahigh energy density, abundance and environmental friendliness. Generating hydrogen by water splitting with highly efficient electrocatalysts is a feasible route to meet current and future energy demand. Herein, the effects of Ru doping and phosphorization treatment on Co₃O₄ nanoarrays for water splitting are systemically investigated. The results show that a small amount of phosphorus can accelerate hydrogen evolution reaction (HER) and the trace of Ru dopant can significantly enhance the catalytic activities for HER and oxygen evolution reaction (OER). Ru-doped cobalt phosphorous oxide/nickel foam (CoRuPO/NF) nanoarrays exhibit highly efficient catalytic performance with an overpotential of 26 mV at 10 mA cm⁻² for HER and 342 mV at 50 mA cm⁻² for OER in 1 M KOH solution, indicating superior water splitting performance. Furthermore, the CoRuPO/NF also exhibits eminent and durable activities for alkaline seawater electrolysis. This work significantly advances the development of seawater splitting for hydrogen generation.

Received 6th March 2020

Accepted 7th July 2020

DOI: 10.1039/d0ra02128h

rsc.li/rsc-advances

1. Introduction

In recent years, the excessive consumption of fossil fuels has brought various environmental problems, such as greenhouse effect, smog or acid rain. Therefore, it is necessary to develop clean renewable energy sources as viable alternatives to fossil-based energy. Among all the known alternative sources of energy, hydrogen is a clean and renewable energy source with no by-products affecting the environment and no carbon release, promising to address future energy demand.^{1–6}

A promising method for generating hydrogen is direct electrolysis of water using electricity derived from solar or wind energy.^{7,8} This method is not only environmental friendly, but also cost-effective, as water exists in abundant quantity in nature.^{9–11} For the process of electrolyzing water, the electrocatalysts for hydrogen evolution reaction (HER) and oxygen evolution reaction (OER) play a critical role to improve the conversion efficiency.^{12,13} At present, platinum and ruthenium/iridium are ideal for HER and OER respectively.^{14,15} However, the high cost and scarcity of noble metals limit the large-scale

application and commercialization of hydrogen energy.¹⁶ Thus, it is important to develop highly efficient electrocatalysts with low-cost and abundant sources in nature. Group VIII transition metals (TMs) and their oxides (TMOs) can serve as efficient catalysts for water electrolysis owing to their unique 3d electronic structure. Additionally, their low-cost and abundant reservoirs in nature makes them ideal for the large-scale water-splitting.¹⁷ Nickel foam (NF) is able to be introduced as the substrate for the growth of TMOs due to their strong interaction with each other and prominent specific surface area.¹⁸ The unique TMO/NF heterostructure can facilitate the charge transfer from NF electrode to surface active site.¹⁹ Moreover, the incorporating heteroatoms such as P, S, and Se in the TMOs can further improve the overall performance of the TMOs based catalysts by modulating the electronic structures of active sites.^{2,11,20} The transition metal phosphides (TMPs) exhibit outstanding performance of water splitting in alkaline solution. Wang *et al.* reported that the P-doped Co₃O₄/NF nanowires exhibit superior performance in HER.²¹ In addition, doping with trace of noble metal in TMPs can further improve the catalytic activities during water splitting process. Studies have shown that decorating TMOs with Ru as a dopant is an effective way to further enhance the catalytic activity of TMO's for its significantly similar hydrogen bond strength as Pt, which can considerably boost the catalytic activity in an alkaline solution.^{22–24} Furthermore, most investigations of water splitting are carried out in the aqueous solution originated from ultrapure water, which would increase the difficulty of developing

^aSchool of Materials and Energy, University of Electronic Science and Technology of China, Chengdu, 610054, PR China. E-mail: hainingji@uestc.edu.cn; xbnui@uestc.edu.cn

^bInstitute of Fundamental and Frontier Sciences, University of Electronic Science and Technology of China, Chengdu, 610054, PR China

† Electronic supplementary information (ESI) available. See DOI: 10.1039/d0ra02128h



hydrogen energy in freshwater-deficient area. In order to overcome this issue, Dionigi and co-workers exploited abundant seawater instead of ultrapure water as electrolyte. This can not only save fresh water resources, but also obtain clean potable water from seawater.^{25,26} Unfortunately, the current electrocatalysts have exhibited poor performance in seawater solutions *i.e.* high overpotentials and poor stability compared to ultrapure water as electrolyte.^{27–29} Therefore, it is important to find out new catalysts to address these problems.

In this work, P and Ru co-doped cobalt oxide nanoarrays supported on NF (CoRuPO/NF) is synthesized *via* hydrothermal reaction along with solid phase method. CoRuPO/NF used as a bifunctional catalyst for overall water electrolysis exhibits a very low overpotential of 26 mV at 10 mA cm^{−2} for HER and an overpotential of 342 mV at 50 mA cm^{−2} for the OER in the alkaline electrolyte. In addition, the electrocatalytic performance of CoRuPO/NF in alkaline solution prepared by real seawater (Huangyan Island Beach, South China Sea) are also investigated. The CoRuPO/NF shows enviable chemical stability and catalytic activities in the alkaline seawater electrolyte, making CoRuPO/NF heterostructure a promising electrocatalyst for long-term and sustainable water splitting.

2. Experimental

2.1 Materials

NF was bought from Alantum New Material Technology Co. Ltd. Sodium hypophosphite (NaH₂PO₂), cobaltous nitrate hexahydrate (Co(NO₃)₂·6H₂O), ruthenium trichloride (RuCl₃), KOH and KCl were supplied by Adamas-beat. Urea was purchased from Aladdin Ltd. (Shanghai, China). Ammonium fluoride (NH₄F), HCl as well as ethanol was obtained from Chengdu Kelong Chemicals Co. Ltd. Pt/C (20 wt%) was purchased from Johnson Matthey company. 5 wt% of NafionTM and RuO₂ were from Sigma-Aldrich. Ultrapure water was further purified through a Millipore system. The seawater was obtained from near Huangyan Island Beach, South China Sea. All the chemical reagents used in this experiment were of analytical grade and applied as received without further processing.

2.2 Synthesis

2.2.1 Synthesis of Co₃O₄/NF and CoRuO/NF. CoRuO/NF was synthesized using conventional hydrothermal method.³⁰ NFs were cut into small pieces with dimensions of 2 cm × 4 cm. The NFs were treated with 1 M HCl solution, ethanol and deionized (DI) water sequentially, for 30 minutes in the ultrasonic machine. Co(NO₃)₂·6H₂O (3.32 g), NH₄F (0.84 g), urea (3.42 g) were dissolved into 80 mL of DI water and the mixture was stirred strongly for 30 minutes at the room temperature to form a homogeneous solution. This homogeneous solution along with cleaned NF were transferred into a 100 mL Teflon-lined stainless-steel autoclave. Similarly, Co(NO₃)₂·6H₂O (3.154 g), RuCl₃ (0.1183 g), NH₄F (0.84 g), urea (3.42 g) were poured into 80 mL DI water and the product was stirred in the aforesaid way to obtain homogeneous solution. The obtained solution together with two pieces of dried NFs were also shifted

into similar Teflon-lined stainless-steel autoclave. Subsequently, they were maintained at 120 °C for 6 hours in the electric thermostatic oven. After the heating was over the autoclaves were let to cool down to the room temperature. Finally, the NF samples from both autoclaves were taken out and washed with DI water and ethanol several times sequentially. The washed samples were then placed in a vacuum oven and dried at 60 °C overnight. Afterwards, these samples were placed in the quartz-boats and annealed at 350 °C for 2 hours with a heating ramp rate of 5 °C min^{−1}. Hence, Co₃O₄/NF and CoRuO/NF were obtained and secured for later use.

2.2.2 Synthesis of CoPO/NF and CoRuPO/NF. In order to obtain CoPO/NF or CoRuPO/NF, the above obtained Co₃O₄/NF or CoRuO/NF sample was placed in the quartz-boat on one side with NaH₂PO₂ (200 mg) on the opposite side. The sample was then annealed at 300 °C for 30 min with a heating ramp rate of 2 °C min^{−1} under Ar flow.

2.2.3 Preparation of 20 wt% Pt/C/NF and RuO₂/NF. Samples containing 20 wt% Pt/C/NF and RuO₂/NF were chosen as the benchmark electrocatalysts for comparison of the H₂ and O₂ generation activity following the recipe reported previously.²¹ Briefly, 50 mg of catalyst (20wt% Pt/C or RuO₂) and 10 μL 5wt% NafionTM solution were dispersed in 990 μL 1 : 1 v/v water/ethanol solvent by 30 min sonication to form an ink. Subsequently, 53.4 μL catalyst ink was loaded on NF (0.5 cm × 0.5 cm) and air-dried at room temperature.

2.3 Characterization

2.3.1 Materials characterization. Scanning electron microscope (SEM) was performed on XL30 ESEM FEG at an accelerating voltage of 20 kV. The elemental analysis of the samples was performed by energy dispersive X-ray spectroscopy (EDS), employing XL30 ESEM FEG scanning electron microscope. X-ray diffraction spectra (XRD) were recorded by Bruker D8 Advance diffractometer with CuKα₁ radiation (λ = 0.15406 nm). X-ray photoelectron spectroscopy (XPS) spectra were acquired on Thermo ESCALAB 250. Inductively coupled plasma optical emission spectrometry (ICP-OES) analysis was performed on PerkinElmer 8300.

2.3.2 Electrochemical measurements. All the electrochemical measurements were performed on the CHI760E electrochemical workstation (CH Instruments, Inc., Shanghai) in a standard three-electrode cell system. CoRuPO/NF (active area 2 cm²) was used as the working electrode. A graphite rod was used as counter electrode and Ag/AgCl was employed as the reference electrode. The potentials mentioned in our work were converted to reversible hydrogen electrode (RHE). The temperature of the solvent was maintained at about 25 °C throughout whole experiment. The electrochemical tests for HER are performed after purging the electrolyte with argon gas for 30 min, and the oxygen is saturated in electrolyte for OER test by purging O₂ for 30 min. The catalytic performance for HER was measured by linear sweep voltammetry (LSV) from 0.1 to −0.9 V *vs.* RHE. The catalytic activity toward the OER was evaluated by LSV from 1.1 to 1.9 V *vs.* RHE. All polarization curves were corrected for iR drop throughout the system. The



electrochemical impedance spectroscopy (EIS) was also carried out from the 1 Hz to 10^5 Hz at -0.176 V vs. RHE for HER. The cyclic voltammetry (CV) was performed from 0.12 to 0.26 V vs. RHE at variable rates from 2 to 120 mV s^{-1} . Stability of the HER was checked by chronoamperometric measurements at a constant voltage of -0.11 V vs. RHE for 10 hours.

3. Results and discussion

3.1 Morphology and structure characterization

Nanoarray CoRu(OH)F were grown on the surface of NF *via* a simple hydrothermal method with Ru : Co ratio of 1 : 10. Subsequently, as-prepared CuRu(OH)F nanoarrays were given oxidation and phosphorylation treatment at a mild temperature to obtain CoRuPO/NF electrodes. The schematic illustrations in Fig. 1 demonstrate the synthesis route of CoRuPO/NF. The morphologies of synthesized samples and pristine NF were characterized using SEM. As shown in Fig. 2a, the pristine NF presents macroporous structure with smooth surface. After hydrothermal reaction and oxidation treatment, the Co_3O_4 nanowires grow and fully cover the surface of the NF (Fig. 2b). However, the porous structure of the NF was retained (Fig. S1†). Such a structure is beneficial for the distribution of active sites. When incorporating Ru or P dopants in Co_3O_4 , the morphologies of CoRuPO/NF show no obvious variation and maintain the shape of urchin in Fig. 2c–f. The existence of such a porous nanostructure contributes to expose more active sites and the rapid mass transfer of reactants and products.^{4,17,31,32}

The elemental composition of the samples was studied by EDS. As shown in Fig. 3a, the EDS spectrum of CoRuPO/NF demonstrates the presence of all the necessary elements such

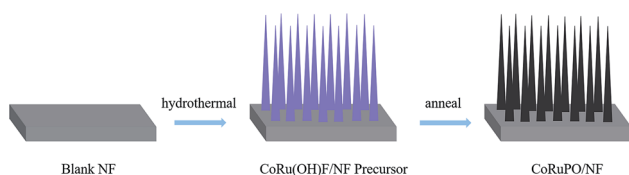


Fig. 1 Schematic illustration of the synthetic process for CoRuPO/NF.

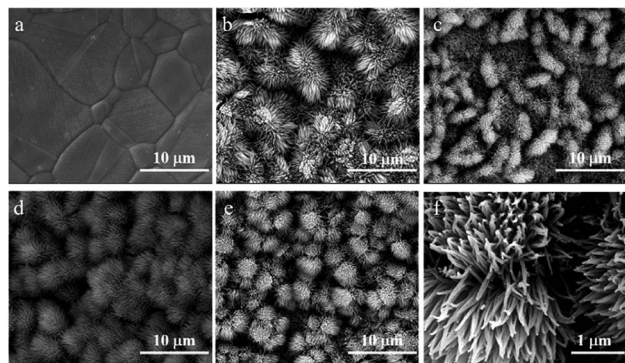


Fig. 2 SEM images of (a) blank NF, (b) Co_3O_4 /NF, (c) CoRuO/NF, (d) CoPO/NF, and (e and f) CoRuPO/NF film at different magnifications.

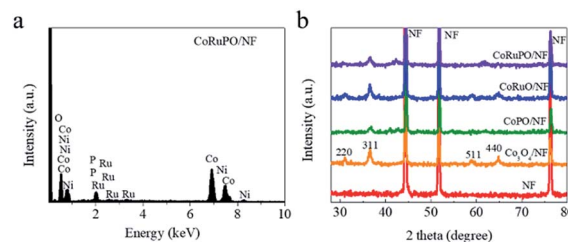


Fig. 3 (a) EDS spectrum of as synthesized CoRuPO/NF catalyst, and (b) XRD patterns of pure NF, Co_3O_4 /NF, CoPO/NF, CoRuO/NF, and CoRuPO/NF.

as Co, P, Ru and O in the CoRuPO/NF, and the composition percentage of the main elements is summarized in Table S1.† The results indicate that Ru and P have been successfully incorporated in the Co_3O_4 nanoarrays (Fig. S2†). XRD was employed to study the crystal structure of samples. As shown in Fig. 3b, the sharp diffraction peaks of CoRuPO/NF at 44.5° , 51.8° and 76.4° correspond to (111), (200) and (220) planes of nickel, owing to the NF substrate. The diffraction peaks located at 31.2° , 38.5° , 59.4° and 67.3° correspond to the (220), (311), (511) and (440) planes of Co_3O_4 respectively.^{21,33,34}

To further determine the elemental composition and chemical states of the samples, XPS was performed. The full survey XPS spectrum of the CoRuPO/NF sample displayed in Fig. 4a clearly demonstrates the presence of Co, Ni, O, C, P and Ru elements, which is consistent with the EDS results in Fig. 3a. Furthermore, the high resolution XPS (HRXPS) spectrum of Co 2p is deconvoluted into four peaks (Fig. 4b). The corresponding subpeaks at 780.9 eV and 796.5 eV can be attributed to Co 2p_{3/2} and Co 2p_{1/2}, respectively. The satellite peaks observed at 795.0 eV and 781.1 eV can be ascribed to Co with oxidation states Co^{3+} and Co^{2+} .^{35–37} The HRXPS spectrum of O 1s reveals three peaks at binding energies of 529.45 eV, 530.18 eV and 531.0 eV, which are attributed to metal–oxygen bonds in the spinel lattice, surface adsorbed oxygen, and O from the surface of absorbed H_2O due to P doping, respectively (Fig. S3†).³⁸ The

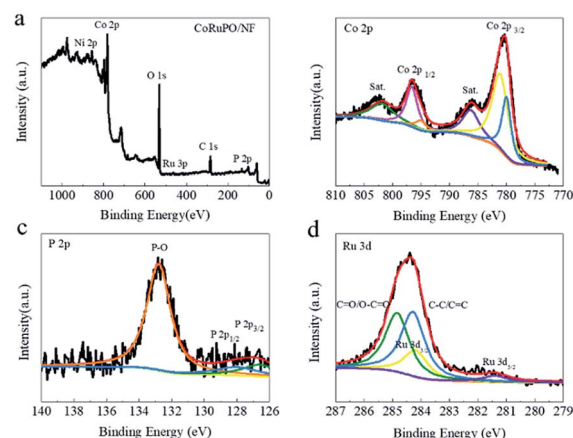


Fig. 4 (a) XPS survey spectrum, high resolution XPS spectra of (b) Co 2p, (c) P 2p, and (d) Ru 3d for CoRuPO/NF.

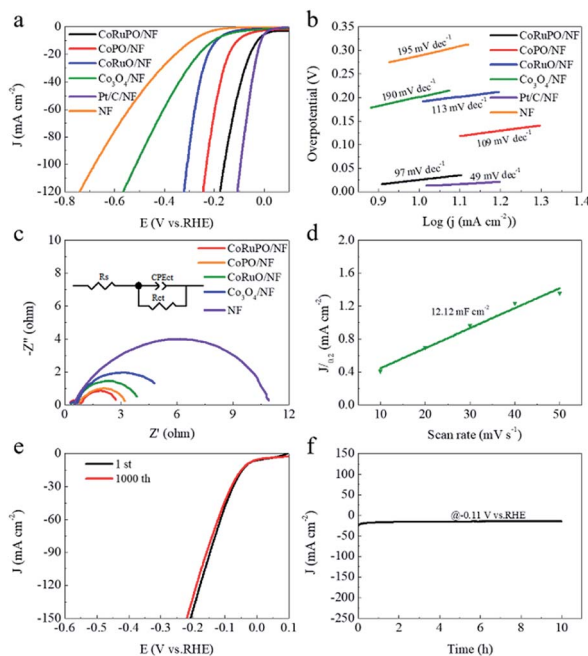


Fig. 5 (a) Polarization curves of NF, $\text{Co}_3\text{O}_4/\text{NF}$, CoRuO/NF , CoPO/NF , CoRuPO/NF , and $\text{Pt}/\text{C}/\text{NF}$ for HER and (b) the corresponding Tafel plots. (c) Nyquist plots for the electrocatalysts. Inset: the equivalent circuit model for the Nyquist plots. (d) Linear fitting of the capacitive currents of the CoRuPO/NF vs. the scan rates. (e) Polarization curves of CoRuPO/NF initially and after 1000 cycles at a scan rate of 10 mV s^{-1} for HER. (f) The chronoamperometry plot of CoRuPO/NF for 10 hours at a constant voltage of -0.11 V vs. RHE.

HRXPS spectrum of P (Fig. 4c) exhibits two peaks at 126.6 eV and 128.0 eV corresponding to $\text{P } 2p_{3/2}$ and $\text{P } 2p_{1/2}$ respectively, and the peak at 132.8 eV can be ascribed to the oxidized phosphate species.^{35,39} The deconvolution of HRXPS spectrum of Ru 3d obtained two peaks at 281.4 eV and 284.2 eV (Fig. 4d), originated from $\text{Ru } 3d_{5/2}$ and $\text{Ru } 3d_{3/2}$ respectively.^{40,41} Comparing the Co 2p and O 1s peaks of CoRuO/NF , CoPO/NF and CoRuPO/NF (Fig. S4†), it can be seen that after the Ru or P is doped, the binding energy changes, which may be due to the alteration in the electron density caused by doping.²¹ The XPS analysis infers the successful synthesis of CoRuPO/NF .

3.2 Electrochemical performance characterization

The electrochemical tests of the samples were carried out in a 1.0 M KOH solution utilizing a standard three-electrode system. Fig. 5a displays the polarization curves of as prepared

Table 1 The comparison for EIS parameters of electrodes

Electrodes	$R_s/\text{ohm cm}^2$	$R_{ct}/\text{ohm cm}^2$
NF	0.635	8.884
$\text{Co}_3\text{O}_4/\text{NF}$	0.251	4.995
CoRuO/NF	0.264	3.483
CoPO/NF	0.278	2.686
CoRuPO/NF	0.206	2.021

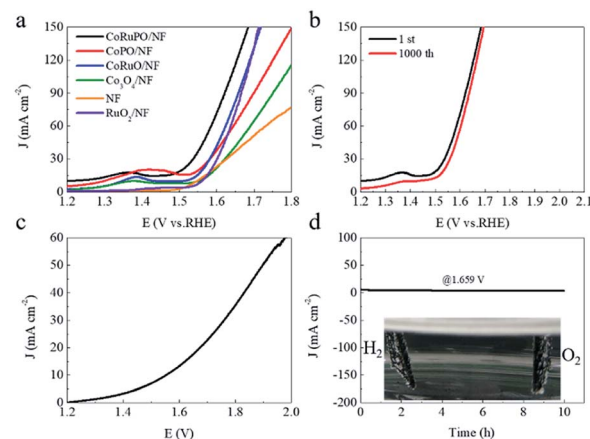


Fig. 6 (a) Polarization curves of NF, $\text{Co}_3\text{O}_4/\text{NF}$, CoRuO/NF , CoPO/NF , CoRuPO/NF , and RuO_2/NF for OER. (b) Polarization curves of CoRuPO/NF initially and after 1000 cycles at a scan rate of 10 mV s^{-1} for OER. (c) Polarization curve of a two-electrode at a sweeping rate of 10 mV s^{-1} for CoRuPO/NF . (d) The chronoamperometry plot of CoRuPO/NF at a stationary voltage of 1.659 V for 10 h.

electrodes with a scan rate of 10 mV s^{-1} , and the corresponding overpotential (η_{10}) obtained at 10 mA cm^{-2} for HER. As expected, the LSV curves of the synthesized electrodes are positively shifted after modification by the Ru and P dopants compared with bare NF. For example, as a substrate material, the η_{10} of NF is 288 mV. The η_{10} of $\text{Co}_3\text{O}_4/\text{NF}$ becomes 202 mV after growing Co_3O_4 nanoarray on the surface NF, suggesting that inducing Co_3O_4 nanoarray is beneficial to improve the activity of electrode. There can be two reasons for this result. First, the intrinsic catalytic activity of Co_3O_4 is higher than that of pristine NF. The second is that nanoarray of Co_3O_4 can magnify the specific surface area of electrodes and lead to more active sites participation for the HER. After decorating Co_3O_4 nanoarray with doping Ru or phosphorization, the catalytic performances of CoRuO/NF and CoPO/NF are improved with a η_{10} of 191 mV and 106 mV, respectively. Surprisingly, the η_{10} of CoRuPO/NF is only 26 mV. This value is higher than the $\text{Pt}/\text{C}/\text{NF}$ (13 mV), but its mass activity is more excellent (as seen in Table S2†). This result is attributed to the strong hydrogen bond strength of Ru atoms, which slows down the hydrogen release and promotes the adsorption and desorption of hydrogen.^{42,43}

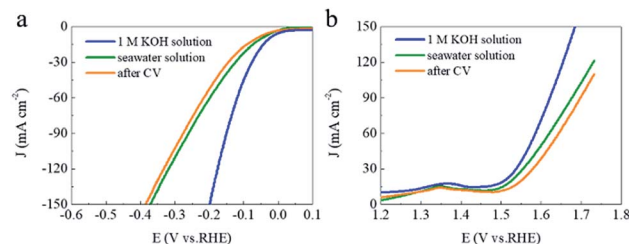


Fig. 7 Polarization curves of CoRuPO/NF in 1.0 M KOH solution, seawater solution and after 1000 CV cycles at a scan rate of 100 mV s^{-1} in seawater + 1.0 M KOH (a) from -0.22 V to 0.12 V vs. RHE for HER, (b) from 1.30 V to 1.60 V vs. RHE for OER.



Table 2 Comparison of electrocatalytic performances of well-developed electrocatalysts for HER

Catalysts	Electrolyte	Overpotential (mV @ mA cm ⁻²)	Ref.
CoRuPO/NF	1 M KOH + natural seawater	62 @ 10	This work
Pt-Ru-Mo	Natural seawater	196 @ 10	51
NiCoP/NF	Natural seawater	287 @ 10	52
Ti/NiPt	Natural seawater	1000 @ 57	53
Ti/NiCo	Natural seawater	1000 @ 172	53

The reaction mechanism and kinetics of as-synthesized catalytic electrodes towards the HER are also evaluated by the Tafel slopes, as depicted in Fig. 5b. CoRuPO/NF exhibited a Tafel slope of 97 mV dec⁻¹, which is higher than Pt/C (49 mV dec⁻¹), suggesting that it is still slightly inferior to Pt/C/NF in kinetics. However, compared with the CoPO/NF and CoRuO/NF, the Tafel slope is lower indicating the favorable HER kinetics for the CoRuPO/NF based electrode is a Volmer–Heyrovsky route. The incorporation of Ru and P changes the electron density around Co, causing a part of Co²⁺ to Co³⁺, thereby generating enriched empty d orbitals. The empty d orbitals can promote the adsorption of OH groups and H atoms to improve the kinetics of the Volmer step.^{44,45} Doping Ru and P in Co₃O₄ nanoarray is an effective way to enhance the HER performance.

In order to investigate the interfacial reactions and the electrode kinetics for HER, we performed EIS for the samples. The Nyquist diagram in Fig. 5c presents semicircles and the corresponding electrochemical parameters are summarized in Table 1. Moreover, the equivalent circuit is represented in the inset of Fig. 5c. The charge transfer resistance (R_{ct}) between the CoRuPO/NF catalyst based electrode and electrolyte interface is lowest (2.021 ohm cm²), indicating a fast electron transfer rate and rapid electrocatalytic kinetics for HER.⁴⁶ Fig. 5d displays the CV curves of CoRuPO/NF with different scan rates, and the corresponding double layer capacitance (C_{dl}) is 12.12 mF cm⁻² via an archetypical CV method.^{47,48} The electrochemical active surface area (ECSA) was estimated by C_{dl} according to the formula presented in eqn (1) below.⁴⁹

$$ECSA = C_{dl}/C_s \quad (1)$$

where C_s is the specific capacitance in 1 M KOH solution with a value of 0.040 mF cm⁻².⁵⁰ Therefore, the value of ECSA was estimated as 303 cm², which is advantageous for electrochemical activity of HER.

The long-term stability is another key factor to evaluate an electrocatalyst for the sustainable energy conversion. Firstly, we probed the stability of the CoRuPO/NF based electrode by performing CV scan between -0.22 and +0.12 V vs. RHE at a scan rate of 100 mV s⁻¹ in 1.0 M KOH as electrolyte. After 1000 CV cycles, the polarization curve is almost overlapping the initial ones (Fig. 5e). Moreover, the current vs. time ($i-t$) curve of CoRuPO/NF electrode is carried out by chronoamperometry measurement for 10 hours at a constant voltage of -0.11 V vs. RHE. As shown in Fig. 5f, the current density has no significant phase change compared with the initial current density after 10 hours of continuous large current operation, demonstrating excellent stability of CoRuPO/NF electrode.

The OER catalytic performance of prepared catalysts were also analyzed for estimating the bifunctional activities for water electrolysis. Although the LSV curves did not display the same behavior for OER compared to HER, it can be seen that the overpotential of CoRuPO/NF for OER is only 342 mV to reach 50 mA cm⁻² (see Fig. 6a), which is better than RuO₂/NF (397 mV). Meanwhile, the mass activity of CoRuPO/NF is as high as 1192 mA mg⁻¹ at the overpotential of 250 mV vs. RHE, which is 4 times relative to RuO₂/NF (Table S3†). Doping Ru and P is an effective way to adjust the electronic structure and enhance the electrochemical performance. Moreover, the synergistic effect between Ru and Co can ameliorate the conductivity of Co₃O₄ to improve the catalytic activities for OER.^{56,57} In addition, the LSV curve of CoRuPO/NF changes slightly after treated by CV scan with 1000 cycles. Based on the above results, it can be concluded that CoRuPO/NF can serve as the bifunctional electrocatalyst for overall water electrolysis. A two-electrode system in which CoRuPO/NF sheets deployed both as anode and cathode is assembled to further monitor the performance of full water splitting. As shown in Fig. 6c, a current density of 10 mA cm⁻² is obtained at a voltage of 1.56 V, indicating a low potential in favour of water electrolysis.⁵⁸ This result is attributed to the

Table 3 Comparison of electrocatalytic performances of well-developed electrocatalysts for OER

Catalysts	Electrolyte	Overpotential (mV @ mA cm ⁻²)	Ref.
CoRuPO/NF	1 M KOH + natural seawater	69 @ 10	This work
NiMoN@NiFeN	1 M KOH + natural seawater	307 @ 100	29
NiCFPO/C@CC	0.1 M KOH + natural seawater	325 @ 10	54
Co-Fe LDH	Natural seawater	530 @ 10	27
Co-Bi	1 M KBi + natural seawater	550 @ 1	55



superior catalytic activities for HER and OER. The stability measurements in Fig. 6d for 10 hours by chronoamperometry exhibit no obvious loss of current density, revealing the outstanding durability of CoRuPO/NF.

In most of previous researches related to water splitting, the electrolytes were based on ultrapure water or fresh water and rarely from the seawater. Therefore, investigating the seawater splitting is a significant work for developing hydrogen energy in freshwater deficient areas. As shown in Fig. 7a and b, the LSV curves of CoRuPO/NF for HER and OER have obvious shifts in seawater electrolyte compared to those of ultrapure water electrolytes, which is possibly due to the poisoning of impurities in seawater. But its overpotential is superior to that of most previously reported catalysts in natural and alkaline seawater solution (As shown in Tables 2 and 3). In addition, the electrocatalyst CoRuPO/NF displays superior durability in seawater even after 1000 cycles of CV without obvious shift for HER and OER, illustrating that the CoRuPO/NF is an outstanding candidate for direct seawater splitting.

4. Conclusions

The Ru and P decorating Co₃O₄ nanoarrays catalyst supported in NF (CoRuPO/NF) was synthesized using hydrothermal method and post-treatments. SEM images showed nanowire morphology of CoRuPO uniformly distributed on NF substrate. EDS and XPS revealed the presence of all the elements such as Co, Ru, P and O in CoRuPO/NF. XRD revealed high crystalline quality of synthesized CoRuPO/NF. The electrochemical results indicated that doping Ru and P is an effective way to improve the catalytic performance towards HER and OER for their synergistic effect. The CoRuPO/NF exhibited superior HER and OER catalytic activities in alkaline solution as well as marvelous stability. Moreover, the seawater splitting performance of CoRuPO/NF was also studied, and the result indicated that CoRuPO/NF possesses the potential of catalysis for efficient seawater splitting.

Conflicts of interest

There are no conflicts to declare.

Acknowledgements

This work was supported by the National Natural Science Foundation of China (Grant No. 61974014), the National Program on Key Basic Research Project (Grant No. SQ2019YFB220038, 2018YFA0306102), and the Sichuan Science and Technology Program under (Grant No. 2019YJ0202).

References

- 1 Y. Shi and B. Zhang, *Chem. Soc. Rev.*, 2016, **45**, 1529–1541.
- 2 S. Anantharaj, S. R. Ede, K. Sakthikumar, K. Karthick, S. Mishra and S. Kundu, *ACS Catal.*, 2016, **6**, 8069–8097.
- 3 H. Wang, Y. Li, R. Wang, B. He and Y. Gong, *Electrochim. Acta*, 2018, **284**, 504–512.
- 4 J. Yang, C. Cai, Y. Li, L. Gao, H. Guo, B. Wang, B. Pu and X. Niu, *Electrochim. Acta*, 2018, **262**, 48–56.
- 5 M. S. Faber and S. Jin, *Energy Environ. Sci.*, 2014, **7**, 3519–3542.
- 6 M. Zhou, H. L. Wang and S. Guo, *Chem. Soc. Rev.*, 2016, **45**, 1273–1307.
- 7 J. Wang, W. Cui, Q. Liu, Z. Xing, A. M. Asiri and X. Sun, *Adv. Mater.*, 2016, **28**, 215–230.
- 8 A. J. Esswein, M. J. McMurdo, P. N. Ross, A. T. Bell and T. D. Tilley, *J. Phys. Chem. C*, 2009, **113**, 15068–15072.
- 9 M. T. Koper, *Nat. Chem.*, 2013, **5**, 255–256.
- 10 B. D. Stubbett, J. C. Peters and H. B. Gray, *J. Am. Chem. Soc.*, 2011, **133**, 18070–18073.
- 11 X. Zou and Y. Zhang, *Chem. Soc. Rev.*, 2015, **44**, 5148–5180.
- 12 Y. Yan, B. Y. Xia, B. Zhao and X. Wang, *J. Mater. Chem. A*, 2016, **4**, 17587–17603.
- 13 J. Yang, H. Guo, S. Chen, Y. Li, C. Cai, P. Gao, L. Wang, Y. Zhang, R. Sun, X. Niu and Z. Wang, *J. Mater. Chem. A*, 2018, **6**, 13859–13866.
- 14 S. Bai, C. Wang, M. Deng, M. Gong, Y. Bai, J. Jiang and Y. Xiong, *Angew. Chem., Int. Ed.*, 2014, **53**, 12120–12124.
- 15 D.-S. Liu, J. Wu, Y. Wang, H. Ji, L. Gao, X. Tong, M. Usman, P. Yu and Z. Wang, *RSC Adv.*, 2017, **7**, 11987–11997.
- 16 S. Yang, L. Chen, W. Wei, X. Lv and J. Xie, *Appl. Surf. Sci.*, 2019, **476**, 749–756.
- 17 P. Babar, A. Lokhande, H. H. Shin, B. Pawar, M. G. Gang, S. Pawar and J. H. Kim, *Small*, 2018, **14**, 1702568.
- 18 X. Hu, Q. Zhou, P. Cheng, S. Su, X. Wang, X. Gao, G. Zhou, Z. Zhang and J. Liu, *Appl. Surf. Sci.*, 2019, **488**, 326–334.
- 19 C. Zhang, J. Xiao, X. Lv, L. Qian, S. Yuan, S. Wang and P. Lei, *J. Mater. Chem. A*, 2016, **4**, 16516–16523.
- 20 J.-T. Ren, L. Chen, G.-G. Yuan, C.-C. Weng and Z.-Y. Yuan, *Electrochim. Acta*, 2019, **295**, 148–156.
- 21 Z. Wang, H. Liu, R. Ge, X. Ren, J. Ren, D. Yang, L. Zhang and X. Sun, *ACS Catal.*, 2018, **8**, 2236–2241.
- 22 J. Mahmood, F. Li, S. M. Jung, M. S. Okay, I. Ahmad, S. J. Kim, N. Park, H. Y. Jeong and J. B. Baek, *Nat. Nanotechnol.*, 2017, **12**, 441–446.
- 23 K. Yang, P. Xu, Z. Lin, Y. Yang, P. Jiang, C. Wang, S. Liu, S. Gong, L. Hu and Q. Chen, *Small*, 2018, **14**, 1803009.
- 24 J. Zhang, P. Liu, G. Wang, P. Zhang, X. Zhuang, M. CHEN, I. Weidinger and X. Feng, *J. Mater. Chem. A*, 2017, **5**, 25314–25318.
- 25 F. Dionigi, T. Reier, Z. Pawolek, M. Gliech and P. Strasser, *ChemSusChem*, 2016, **9**, 962–972.
- 26 S. Dresp, F. Dionigi, S. Loos, J. Ferreira de Araujo, C. Spöri, M. Gliech, H. Dau and P. Strasser, *Adv. Energy Mater.*, 2018, **8**, 1800338.
- 27 F. Cheng, X. Feng, X. Chen, W. Lin, J. Rong and W. Yang, *Electrochim. Acta*, 2017, **251**, 336–343.
- 28 J. Zheng, *Electrochim. Acta*, 2017, **247**, 381–391.
- 29 L. Yu, Q. Zhu, S. Song, B. McElhenny, D. Wang, C. Wu, Z. Qin, J. Bao, Y. Yu, S. Chen and Z. Ren, *Nat. Commun.*, 2019, **10**, 1–10.
- 30 R. Yuan, L. Hu, P. Yu, H. Wang, Z. Wang and J. Fang, *Chemosphere*, 2018, **198**, 204–215.



- 31 L. Li, L. Song, H. Xue, C. Jiang, B. Gao, H. Gong, W. Xia, X. Fan, H. Guo, T. Wang and J. He, *Carbon*, 2019, **150**, 446–454.
- 32 W. Chang, W. Xue, E. Liu, J. Fan and B. Zhao, *Chem. Eng. J.*, 2019, **362**, 392–401.
- 33 S. Liu, Y. Jiang, M. Yang, M. Zhang, Q. Guo, W. Shen, R. He and M. Li, *Nanoscale*, 2019, **11**, 7959–7966.
- 34 Y. Gong, Y. Lin, Z. Yang, F. Jiao, J. Li and W. Wang, *Appl. Surf. Sci.*, 2019, **476**, 840–849.
- 35 Y.-P. Zhu, Y.-P. Liu, T.-Z. Ren and Z.-Y. Yuan, *Adv. Funct. Mater.*, 2015, **25**, 7337–7347.
- 36 H. Schäfer, D. M. Chevrier, K. Kuepper, P. Zhang, J. Wollschlaeger, D. Daum, M. Steinhart, C. Heß, U. Krupp, K. Müller-Buschbaum, J. Stangl and M. Schmidt, *Energy Environ. Sci.*, 2016, **9**, 2609–2622.
- 37 L. Fu, Z. Liu, Y. Liu, B. Han, P. Hu, L. Cao and D. Zhu, *Adv. Mater.*, 2005, **17**, 217–221.
- 38 X. Wu and K. Scott, *Int. J. Hydrogen Energy*, 2013, **38**, 3123–3129.
- 39 C. Tang, R. Zhang, W. Lu, Z. Wang, D. Liu, S. Hao, G. Du, A. M. Asiri and X. Sun, *Angew. Chem., Int. Ed.*, 2017, **56**, 842–846.
- 40 P.-F. Zhang, Y.-Q. Lu, Y.-J. Wu, Z.-W. Yin, J.-T. Li, Y. Zhou, Y.-H. Hong, Y.-Y. Li, L. Huang and S.-G. Sun, *Chem. Eng. J.*, 2019, **363**, 224–233.
- 41 E. Serra-Pérez, S. Álvarez-Torrellas, V. Ismael Águeda, J. A. Delgado, G. Ovejero and J. García, *Appl. Surf. Sci.*, 2019, **473**, 726–737.
- 42 J. Yang, B. Chen, X. Liu, W. Liu, Z. Li, J. Dong, W. Chen, W. Yan, T. Yao, X. Duan, Y. Wu and Y. Li, *Angew. Chem., Int. Ed.*, 2018, **57**, 9495–9500.
- 43 Z. Pu, I. S. Amiin, Z. Kou, W. Li and S. Mu, *Angew. Chem., Int. Ed.*, 2017, **56**, 11559–11564.
- 44 J. Greeley, T. F. Jaramillo, J. Bonde, I. Chorkendorff and J. K. Nørskov, *Nat. Mater.*, 2006, **5**, 909–913.
- 45 Y. Yang, K. Zhang, H. Lin, X. Li, H. C. Chan, L. Yang and Q. Gao, *ACS Catal.*, 2017, **7**, 2357–2366.
- 46 H. Zhang, X. Li, A. Hähnel, V. Naumann, C. Lin, S. Azimi, S. L. Schweizer, A. W. Maijenburg and R. B. Wehrspohn, *Adv. Funct. Mater.*, 2018, **28**, 1706847.
- 47 L. Peng, J. Shen, L. Zhang, Y. Wang, R. Xiang, J. Li, L. Li and Z. Wei, *J. Mater. Chem. A*, 2017, **5**, 23028–23034.
- 48 Y.-Y. Ma, C.-X. Wu, X.-J. Feng, H.-Q. Tan, L.-K. Yan, Y. Liu, Z.-H. Kang, E.-B. Wang and Y.-G. Li, *Energy Environ. Sci.*, 2017, **10**, 788–798.
- 49 V. Kannan, A. I. Inamdar, S. M. Pawar, H. S. Kim, H. C. Park, H. Kim, H. Im and Y. S. Chae, *ACS Appl. Mater. Interfaces*, 2016, **8**, 17220–17225.
- 50 C. C. McCrory, S. Jung, J. C. Peters and T. F. Jaramillo, *J. Am. Chem. Soc.*, 2013, **135**, 16977–16987.
- 51 H. Li, Q. Tang, B. He and P. Yang, *J. Mater. Chem. A*, 2016, **4**, 6513–6520.
- 52 Q. Lv, J. Han, X. Tan, W. Wang, L. Cao and B. Dong, *ACS Appl. Energy Mater.*, 2019, **2**, 3910–3917.
- 53 Y. Zhang, P. Li, X. Yang, W. Fa and S. Ge, *J. Alloys Compd.*, 2018, **732**, 248–256.
- 54 H. J. Song, H. Yoon, B. Ju, D.-Y. Lee and D.-W. Kim, *ACS Catal.*, 2019, **10**, 702–709.
- 55 A. J. Esswein, Y. Surendranath, S. Y. Reece and D. G. Nocera, *Energy Environ. Sci.*, 2011, **4**, 499–504.
- 56 D. Yang, D. Bhattacharjya, S. N. Inamdar, J. Park and J. Yu, *J. Am. Chem. Soc.*, 2012, **134**, 16127–16130.
- 57 H. Liu, G. Xia, R. Zhang, P. Jiang, J. Chen and Q. Chen, *RSC Adv.*, 2017, **7**, 3686–3694.
- 58 C. Xuan, Z. Peng, K. Xia, J. Wang, W. Xiao, W. Lei, M. Gong, T. Huang and D. Wang, *Electrochim. Acta*, 2017, **258**, 423–432.

